S2 Hunga impacts report observational data supplement

Authors Nathaniel Livesey
Graham Mann
David R. Themens
William Randel

Preface

This data supplement has been compiled to provide descriptions and references for the observational data sets used in the separate chapters of this report. We focus on brief overviews of the measurement characteristics and uncertainties, together with the space-time sampling for the various instruments. Further details can be found in the quoted references. Satellite remote sensing data are grouped together, followed by ground-based and balloon measurements.

S2.1 Satellite remote sensing data

ACE-FTS H_2O and other trace gases

The Atmospheric Chemistry Experiment Fourier Transform Spectrometer (ACE-FTS) provides vertical profiles of numerous atmospheric trace species, based on solar occultation measurements (Bernath, 2017; Boone et al., 2023). Additional information is available at `https://uwaterloo.ca/atmospheric-chemistry-experiment/`.

ACE-FTS has been making atmospheric measurements since February 2004, observing 15 sunrise and 15 sunset occultations per day covering a latitude range of approximately 70° N–S. The latitude sampling progresses slowly over time, and it takes approximately three months to cover the latitude range 70°S–70°N.

Figure S2.1 shows the ACE-FTS sampling pattern during January 2020–August 2023, overlaid on the Hunga water vapour plume as observed by MLS, for reference. The instrument measures atmospheric absorption spectra between 750 cm^{-1} to 4400 cm^{-1} at a spectral resolution of 0.02 cm^{-1}; volumetric mixing ratio profiles of more than 40 trace gases can be inferred from these spectra. The vertical resolution of the abundance measurements is approximately 3 km, and atmospheric retrievals are provided on an oversampled 1 km vertical grid. Data used here are from the Version 5 retrievals of ACE-FTS. Data quality flags for all species are used to appropriately screen data quality.

Aura Microwave Limb Sounder (MLS) trace gases and temperature

The Microwave Limb Sounder (MLS), launched on NASA's Aura mission in 2004, measures vertical profiles of a range of trace gases from the upper troposphere to the mesosphere on a daily near-global basis (Waters et al., 2006). MLS vertically scans the atmospheric limb in front of the Aura spacecraft roughly twice per minute and measures thermal emission in the 118, 190, 240, and 640 GHz spectral regions (the Aura MLS 2.5 THz observations have not been made since 2014). Measurements can be made both day and night, including in regions of significant aerosol loading and all but the thickest clouds. At the time of writing, it is anticipated that Aura MLS will continue observing until around May 2026, at which point reduced power availability will dictate the end of the Aura mission.

Starting in May 2024, the MLS "190 GHz" subsystem, which measures H_2O, N_2O, HCN, and upper stratospheric HNO_3, has only been operated for roughly one week each month in order to conserve remaining life for this subsystem, which is showing signs of aging. MLS measurements of other species (e.g., O_3, CO, ClO, HCl, etc.) continue to be made on an uninterrupted basis.

Findings in this report are derived from MLS "Level 2" data—vertical profiles of composition and temperature along the Aura orbit track, with around 3500 profiles reported per day for each product. The vertical coordinate is pressure, and profiles are spaced every 1.5° (approximately 165 km) along the orbit track. Typical vertical resolutions for retrieved profiles range over 2–5 km, depending on the product and altitude region. Published studies of the Hunga eruption and its impacts discussed in this report have used a combination of MLS Version 4 (Livesey et al., 2020) and Version 5 (Livesey et al., 2022) data.

In general, the Version 5 data are recommended over Version 4, particularly for studies involving the water vapour (H_2O) and nitrous oxide (N_2O) products, as a slow change in behaviour of the MLS 190 GHz receiver (likely related to the aging issues discussed above) resulted in observable and statistically significant drifts in these products in the Version 4 dataset (Hurst et al., 2016). The drifts are around 2–10% per decade (Livesey et al., 2021), depending on (1) pressure level, with the strongest drifts seen in the lower stratosphere, (2) species, with N_2O more strongly affected than H_2O, and (3) the basis of comparison (with comparisons to ACE-FTS showing about half as much drift as seen in comparisons to in-situ frost-point sondes).

The Version 5 algorithms and software correct for the slow instrumental changes such that no statistically significant drift is seen in comparisons between MLS and ACE-FTS H_2O, although drifts remain in N_2O and in comparisons of H_2O to the frost-point record.

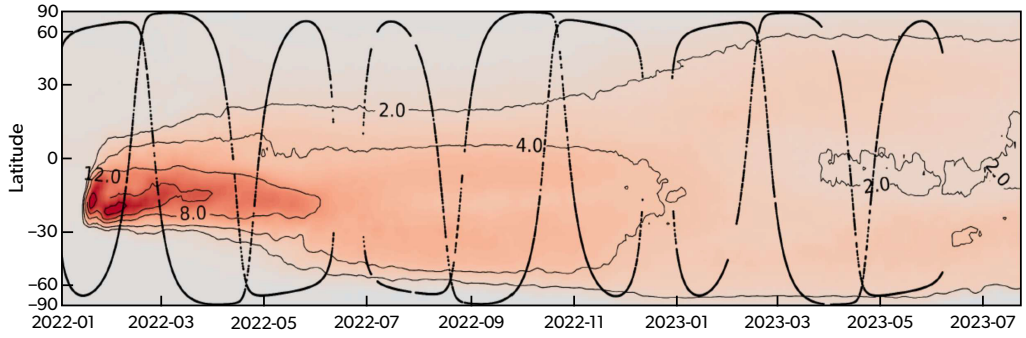

Figure S2.1: *ACE-FTS sampling locations during January 2020–August 2023 overlaying the Hunga water vapour plume as observed by MLS, as a function of time and latitude. The water vapour is expressed in terms of vertically integrated mass (Tg) over 100–1 hPa, calculated in 2.5° latitude bins using anomalies from the 2004–2021 average MLS background. Figure courtesy of Jon Starr at NSF NCAR.*

The only case where the MLS Version 4 data are recommended over Version 5 is in the immediate aftermath (within 2–3 weeks) of the Hunga eruption (Millán et al., 2022). During this period, the strong abundances of H_2O and SO_2 in the core of the stratospheric plume were larger than any seen before in the MLS record. These gave rise to microwave spectra that were very different from those for which the MLS retrievals are designed and optimised. The retrieval algorithms were not able to fit these spectra as well as is typical, resulting in many of the most Hunga-affected profiles being marked as unsuitable for scientific use. Extensive study of this period by the MLS team has concluded that (1) owing to subtle differences in the respective retrieval algorithms, the older Version 4 data are recommended over Version 5 in this specific case, and (2) in this one specific circumstance (and no other), users may waive consideration of the MLS data quality flags and use profiles marked "do not use."

CALIOP space-borne lidar

The Cloud-Aerosol Lidar with Orthogonal Polarization (CALIOP) space-borne lidar (Winker et al., 2007) was launched on the NASA Cloud-Aerosol Lidar and Infrared Pathfinder Satellite Observations (CALIPSO) satellite in April 2006; observations ceased in July 2023. Together with other satellites in the NASA A-train constellation (Stephens et al., 2002), CALIPSO flew in a 705 km altitude sun-synchronous polar orbit with equator-crossing times of about 01:30 and 13:30 local solar time, with the polar orbit ground-track repeating every 16 days.

The CALIOP lidar provided high vertical-resolution measurements of the Hunga aerosol cloud (e.g., Legras et al., 2022; Khaykin et al., 2022), and measurements of polar stratospheric clouds (PSCs) (Pitts et al., 2018), along with a wide range of other aerosol and cloud information over its mission lifetime. The CALIOP PSC type classification followed algorithms developed and validated for ground-based lidar (e.g., Adriani et al., 2004).

Aerosol scattering ratio and derived optical depth The CALIOP lidar measures backscattered light from two lasers, emitting at 532 nm and 1064 nm, with the two principal measurement quantities being total backscatter and backscatter ratio (referred to in this report as the "scattering ratio"). The latter represents the ratio of total backscatter to that from an aerosol-free atmosphere (i.e., total backscatter to Rayleigh backscatter), and thus quantifies the relative enhancement due to aerosol (or clouds).

Figures in this report mainly show backscatter ratio rather than extinction or optical depth, because derivation of the latter quantities hinges on an aerosol-type-dependent conversion from aerosol backscatter to aerosol extinction (and thence optical depth). In practice, such conversions require the assumption of an aerosol "extinction-to-backscatter ratio" – sometimes referred to as the "lidar ratio" (see, e.g., Antuña-Marrero et al., 2021 and section 1 of the supplement to Dhomse et al., 2020) – an unsafe assumption in the Hunga plume, where aerosol properties are poorly known.

The CALIOP aerosol type algorithms (Young et al., 2013) are designed to identify a specific aerosol classification that can be used to ascribe a corresponding lidar ratio, and the retrieval methods include a stratospheric aerosol type (e.g., Kar et al., 2019). For Version 4.2 of the CALIOP aerosol-type retrievals (Tackett et al., 2023), a sub-typing of the stratospheric

aerosol better resolves periods of enhanced smoke aerosol from strong PyroCb events (e.g., Khaykin et al., 2018).

During strong volcanically elevated stratospheric conditions, variations in aerosol particle size distribution modify the extinction-to-backscatter ratio, as seen, for example, by Vaughan et al. (1994) in their analysis of ground-based lidar measurements taken following the 1991 Pinatubo eruption. Research has also employed CALIOP measurements to assess individual eruptions for their varying volcanic sulfate and ash mix (e.g., Prata et al., 2017).

Even for the relatively moderate and low-ash Hunga aerosol, the substantial range in effective radius (e.g., 0.25 – 0.40 μm; Duchamp et al., 2023) affects derived aerosol optical depth from CALIOP during this period. For Pinatubo, tabulated time-varying lidar ratios (e.g., Jäger and Deshler, 2002) have been used to derive aerosol extinction from ground-based lidar backscatter ratio consistently with progressing aerosol microphysical properties (e.g., Shallcross, 2020).

Analyses of derived optical depths from CALIOP (Kim et al., 2018; Ryan et al., 2024) have indicated a general low bias compared to other observations. It is important to note that CALIOP only retrieves aerosol extinction where the particulate attenuated backscatter exceeds the layer detection thresholds (Young and Vaughan, 2009).

CALIOP depolarisation The detector for the CALIOP 532 nm channel is configured to separately measure the parallel and perpendicular polarised backscatter. The ratio of the two is referred to as "depolarisation," expressed either as a percentage or fraction. A large depolarisation value indicates non-spherical particles. This measure is a key discriminator for different types of PSCs (e.g., Adriani et al., 2004), with low depolarisation indicating spherical particles—either liquid aerosol or ternary solution "Type-1b" PSCs—with a stronger backscatter indicating the latter. More highly depolarised backscatter is indicative of either "Type-2" (solid ice) or "Type-1a" (solid nitric acid trihydrate, NAT) PSCs.

Based on the depolarisation information, the CALIOP lidar backscatter measurements can be subsampled to exclude Type-2 (ice) and Type-1a (solid NAT) PSCs, enabling the quantification of backscatter from liquid particles (sulfate aerosol and Type-1b PSCs). The liquid Type-1b PSCs are supercooled ternary solution (STS) droplets that have formed at low temperatures (approximately 3 K below the threshold for NAT PSC formation), growing much larger from the uptake of nitric acid vapour and additional water vapour into existing "binary-solution" sulfuric acid aerosol particles (e.g., Carslaw et al., 1994; Carslaw et al., 1995).

GloSSAC aerosol extinction

The Global Space-based Stratospheric Aerosol Climatology (GloSSAC) was developed in 2018 to provide a best-estimate global dataset for variations in the stratospheric aerosol layer. The main driver for GloSSAC was to provide a stratospheric aerosol dataset for climate models within the CMIP6 (Coupled Model Intercomparison Project phase 6; Eyring et al., 2016) project, and also for use within chemistry–climate models in the CCMI initiative (Chemistry–Climate Modeling Initiative; Morgenstern et al., 2017).

GloSSAC builds on earlier global gridded stratospheric aerosol datasets, notably the Pinatubo "gap-filled dataset" generated for the SPARC ASAP report (Assessment of Stratospheric Aerosol Properties; SPARC, 2006) that was geared primarily to provide Surface Area Density (SAD) information (e.g., Thomason et al., 1997; Thomason et al., 2008) for chemistry–climate models (CCMs) to represent volcanic impacts on the ozone layer (CCM-Val and CCM-Val2, see, e.g., Eyring et al., 2005).

The GloSSAC product is a global and gap-free dataset providing aerosol extinction coefficients at two reference wavelengths (525 and 1020 nm). The 2018 version dataset incorporates an improved post-Pinatubo gap-filling approach (for 1991–1993) that combines the lidar-aligned SAGE-II with data from the Cryogenic Limb Array Etalon Spectrometer (CLAES) on NASA's Upper Atmosphere Research Satellite to fill any gaps. The global dataset also used an approach to address the SAGE-II gap at wintertime high latitudes via equivalent latitude, which is a polar-vortex-oriented coordinate system. For the 2005–2017 period between the end of SAGE-II and the start of SAGE-III/ISS, the v1.0 GloSSAC dataset is primarily based on a merge of the 750 nm OSIRIS aerosol extinction with the 532 nm CALIOP aerosol extinction.

Results discussed in this report are taken from the latest v2.2 GloSSAC record (Kovilakam et al., 2025). This incorporates the latest v5.3 SAGE retrieval and OSIRIS version 7.2, rather than the version 5.07 used in GloSSAC v1.0. GloSSAC v2.2 also benefits from key advances made during the development of the earlier v2.0 dataset, including an improved monthly clima-

tology of Ångström exponent (used for converting OSIRIS extinction to 525 nm) and improved conversion of CALIOP 532 nm backscatter coefficient to 532 nm aerosol extinction (see Kovilakam et al., 2020).

IASI (Infrared Atmospheric Sounding Interferometer) SO_2 and sulfate aerosol

Information on the IASI observations is taken from Sellitto et al. (2024). The RAL (Rutherford Appleton Laboratory) Infrared/Microwave Sounder (IMS) retrieval core scheme (Siddans, 2019) uses an optimal estimation spectral fitting procedure to retrieve atmospheric and surface parameters jointly from co-located measurements by IASI, AMSU (Advanced Microwave Sounding Unit), and MHS (Microwave Humidity Sounder) on the MetOp-B spacecraft, using RTTOV-12 (Radiative Transfer for TOVS; Saunders et al., 2018) as the forward radiative transfer model.

The use of RTTOV-12 enables the quantitative retrieval of sulfate aerosols (SA) and trace gases (SO_2); the bulk of the information on SO_2 and SA in the IMS scheme comes from the IASI observations (Clerbaux et al., 2009). The IMS scheme simultaneously retrieves SO_2 and SA spectroscopic information, which is crucial for avoiding the large uncertainties on both due to their co-existence in volcanic plumes and overlapping spectral signatures (Sellitto et al., 2019). Total uncertainties in individual IMS SO_2 and SA retrievals are estimated at 0.3 DU (SO_2) and 0.002 (SA optical depth) (Siddans, 2023).

MISR aerosol extinction

The Multi-angle Imaging Spectro-Radiometer (MISR) instrument was launched aboard the NASA Terra satellite in December 1999 (e.g., Kahn et al., 2005; Limbacher et al., 2022) and measures upwelling shortwave radiance in four spectral bands centred at 446, 558, 672, and 866 nm. The instrument design has nine viewing angles and derives additional aerosol characterisation information (e.g., Kahn et al., 2010), for example regarding light absorption and particle sphericity, and has developed a sophisticated typology algorithm from the multi-wavelength information (e.g., Kahn and Gaitley, 2015).

From analysis of the MISR products during the initial Hunga aerosol plume (Kahn et al., 2024), the volcanic aerosol was predominantly spherical and non-absorbing, except for the earliest phase of the cloud monitoring. This initial monitoring (21 January 2022) showed that the main northern portion of the plume had a substantially absorbing and non-spherical signature, consistent with that seen in the 23 and 26 January LOAC observations from La Réunion (Kloss et al., 2022), this being during the 10-day period when CALIOP could not measure due to a solar flare (personal communication D. Winker, NASA LaRC).

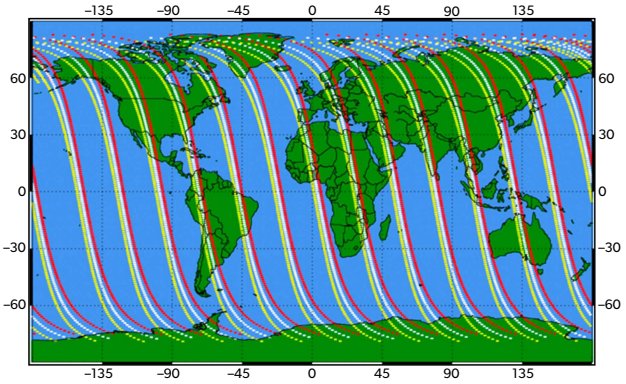

Figure S2.2: *OMPS-LP daily coverage from the S–NPP satellite, illustrating retrieval locations for the left and right slits (red and yellow circles) relative to the central slit (white circles) following the main orbital path. Figure adapted from Loughman et al. (2018).*

OMPS-LP aerosol extinction

The Ozone Mapping and Profile Suite Limb Profiler (OMPS-LP; Loughman et al., 2018; Taha et al., 2021) is a component of the Suomi National Polar-orbiting Partnership (NPP) satellite, launched in October 2011. A second OMPS-LP instrument is now operational on the NOAA-21 mission, launched in 2022, and further launches are planned. OMPS-LP uses a limb-scatter technique to retrieve vertical profiles of aerosol extinction at multiple wavelengths, alongside ozone retrievals. The vertical resolution is approximately 1–2 km. The S–NPP satellite is in a sun-synchronous orbit and provides more than 7000 profiles per day (Figure S2.2). Although OMPS-LP has three vertical slits that make measurements separated horizontally in the cross-track direction by 250 km, only the centre slit, which has the best stray-light performance, is used in the retrievals analysed here.

There are several different retrievals of aerosol extinction from OMPS-LP measurements available, offering somewhat different results. The "NASA OMPS" v2.1 retrieval from the NASA GSFC team uses a single image of the limb radiance to perform a one-dimensional (altitude) retrieval for aerosol extinction. This is performed for six spectral bands spanning 510–997 nm, and profiles are reported from cloud top to 38 km (Taha et al., 2021). The basic approach, which requires an assumption of the particle size distribu-

tion to derive the scattering phase function, follows from the original algorithm developed for limb-scatter aerosol retrievals using OSIRIS measurements (Bourassa et al., 2007). The OMPS v2.1 uses a model-derived gamma function particle size distribution (Chen et al., 2018).

Near the completion of this report, an updated version (v2.5) of NASA OMPS has become available. The v2.5 algorithm improves convergence by increasing the number of iterations, enhancing retrieval performance. Short-wavelength aerosol profiles at 510, 600, 675, and 745 nm were filtered for unrealistic values (mainly at lower altitudes and large scattering angles) using the colour ratio relative to 869 nm. Additional filtering removed profiles with extinction greater than 0.1 km^{-1} or retrieval residuals greater than 50%. Compared with v2.1, v2.5 aligns more closely with GloSSAC data (see Figure S2.3) and captures a pronounced SAOD maximum in late January–early February 2022, linked to rapid SO_2-to-SO_4 conversion in the Hunga cloud driven by elevated water vapour. This feature is absent in both GloSSAC and SAGE records.

A separate retrieval of OMPS-LP is available from the University of Saskatchewan (Bourassa et al., 2023), known as the USASK product. The USASK retrieval employs a tomographic method (Degenstein et al., 2003) to improve limb-scattering aerosol extinction retrievals, as described in Zawada et al. (2018). The tomographic two-dimensional inversion combines successive limb images from the OMPS-LP central slit. Aerosol extinction is reported at 745 nm on a retrieval grid of 1 km vertically and 125 km horizontally, which approximately matches the OMPS-LP sampling. A single-mode lognormal particle size distribution is assumed. The USASK retrieval improved characterisation of some early-phase Hunga aerosol layers (Bourassa et al., 2023) compared to the v2.1 NASA OMPS-LP aerosol extinction.

Although an additional OMPS-LP aerosol product developed by the University of Bremen (IUP) is available (Rozanov et al., 2024), those data are not used for analysis in this report but are included in the measurement uncertainty discussion in Chapter 3.

OSIRIS aerosol extinction

The Optical Spectrograph and Infrared Imager System (OSIRIS) is a limb-scatter instrument launched aboard the Odin satellite in 2001 that continues to operate at the time of writing. The Optical Spectrograph (OS) is the primary instrument, measuring scattered

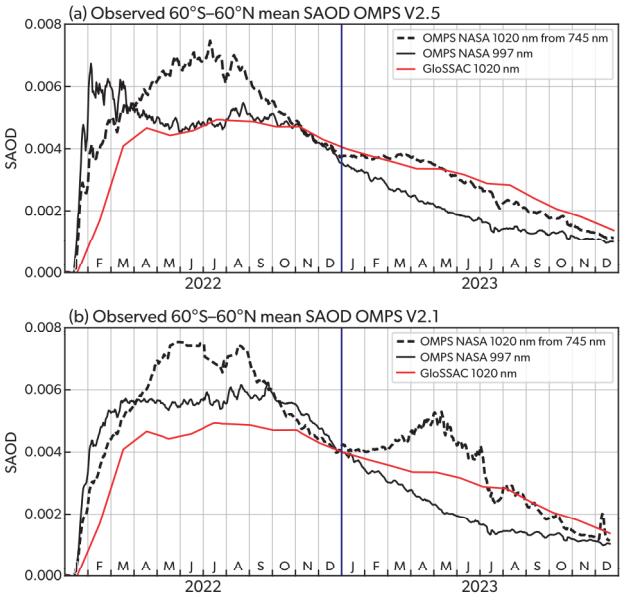

Figure S2.3: *Comparisons of near-global average (60°S–60°N) stratospheric aerosol optical depths (SAOD) from OMPS v2.1, v2.5, and GloSSAC. SAOD for the first two years after the Hunga eruption are shown with background SAOD removed. (a) NASA OMPS-LP v2.5 1020 nm values are derived by converting 745 nm SAOD using the SAGE III/ISS 745-to-1020 nm Ångström exponent; NASA OMPS-LP v2.5 997 nm SAOD shown directly, without any conversion, and GloSSAC 1020 nm SAOD. (b) NASA OMPS-LP v2.1 1020 nm values are derived by converting 745 nm SAOD using the same SAGE III/ISS Ångström exponent; NASA OMPS-LP v2.1 997 nm SAOD shown directly, without any conversion, and GloSSAC 1020 nm SAOD.*

sunlight between 284 and 810 nm with approximately 1.0 nm spectral resolution. The OSIRIS inversion retrieves aerosol extinction at 750 nm on a 1 km grid, with the profile information having approximately 2 km vertical resolution (Bourassa et al., 2007). The inversion requires an assumption of the particle size distribution to derive the scattering phase function. The OSIRIS sampling generally provides between 100 and 400 profiles per day over 82°S–82°N (excluding polar night), depending on the time of year, with a slight bias toward the Northern Hemisphere.

Radio occultation stratospheric H_2O

Radio Occultation (RO) measures the bending angle of radio waves propagating through the atmosphere, from which vertical profiles of atmospheric refractivity (N) can be derived with high vertical resolution (approximately 1 km). The refractivity is dependent primarily on temperature and water vapour (H_2O) in

the atmosphere according to:

$$N = 77.6\left(\frac{p}{T}\right) + 3.73 \times 10^5\left(\frac{e}{T^2}\right), \qquad \text{(S2.1)}$$

where p is pressure, T is temperature, and e is H_2O partial pressure.

Under normal conditions, the H_2O term makes virtually no contribution to N at altitudes above 10 km, and thus H_2O is not detectable by RO measurements in the stratosphere. However, in the case of extremely large stratospheric H_2O concentrations in the early Hunga plume (>1000 ppmv), the RO measurements can be combined with independent temperature observations to derive estimates of stratospheric H_2O. Details of these calculations are described in Khaykin et al. (2022) and Randel et al. (2023).

Radio occultation ionospheric electron density profiles

Radio occultation also measures the phase advance and group delay on two Global Navigation Satellite System (GNSS) frequencies, which—like ground-based GNSS measurements—can be used to measure the path-integrated electron density of the ionosphere between the transmitter and receiver satellites. During occultations, time series of this path-integrated electron density can then be inverted using an Abel transform to derive profiles of the ionospheric electron density. These profiles are often attributed to the tangent point of the occultation measurement and are frequently used for ionospheric event remote sensing (Syndergaard et al., 2006).

Some limitations of the technique are discussed in Shaikh et al. (2014), Pedatella et al. (2015), and Currie et al. (2021).

SAGE III/ISS

Water vapour and ozone The Stratospheric Aerosol and Gas Experiment (SAGE) III provides stratospheric water vapour, ozone, nitrogen dioxide, and aerosol extinction coefficient profiles using solar occultation observations from the International Space Station (ISS). SAGE III/ISS is in a mid-inclination orbit (51.6°) and provides 15 sunrise and 15 sunset measurements per day, covering the latitude range between 50°S and 50°N for most months of the year. The latitude sampling progresses slowly over time, such that it takes approximately one month to cover the latitude range 50° N–S.

Figure S2.4 shows the sampling of SAGE III/ISS during January 2020–August 2023, overlaying the Hunga H_2O plume observed by MLS for reference. Data used here are based on retrieval version v5.2. The vertical resolution of all data products is approximately 0.75 km, with profile retrievals reported on a 0.5 km grid.

The trace gas profile data are provided in units of number density on altitude and are converted to mixing ratio using the temperature and pressure profiles reported in the SAGE III/ISS data files, which originate from the Modern-Era Retrospective Analysis for Research and Applications, Version 2 (MERRA-2; Gelaro et al., 2017).

Data quality for the v5.1 retrieval of the SAGE III/ISS ozone data (the "AO3" product) is discussed in Wang et al. (2020). Water vapour retrievals for v5.1 were validated in Davis et al. (2021) and Park et al. (2021).

Aerosol extinction and derived aerosol parameters SAGE III/ISS also measures aerosol extinction at nine wavelengths (384, 449, 521, 602, 676, 756, 864, 1022, and 1544 nm). By directly measuring the extinction of the solar radiation, SAGE III/ISS provides measurements with high accuracy and precision (Thomason et al., 2021). The vertical resolution is approximately 1 km, with profiles reported in 0.5 km increments from 0.5 to 40 km altitude (Damadeo et al., 2013).

The "half-to-one-micron extinction ratio" gives a general indicator of variations in particle size distribution (e.g., Thomason et al., 2021) based on the mid-visible (525 nm) to near-infrared (1020 nm) SAGE-II aerosol extinctions. The multi-wavelength aerosol extinction coefficient measurements also provide derived aerosol parameters for variations in the stratospheric aerosol layer particle size distribution (Thomason et al., 2008; Knepp et al., 2024), within limitations discussed by Savigny and Hoffmann (2020).

The latest v5.3 SAGE III/ISS data release includes, for the first time, a suite of aerosol size distribution parameters (Knepp et al., 2024). Applying the so-called "three-lambda method" (Thomason et al., 2008), the approach relates aerosol extinction at three wavelengths to aerosol surface area density (SAD) and volume concentration, the ratio of the latter to the former then providing the effective radius.

The aerosol particle size distribution is a key factor driving the radiative and stratospheric chemistry impacts of major volcanic eruptions, and variants on the three-lambda method have been applied to generate global datasets for coordinated chemistry–climate

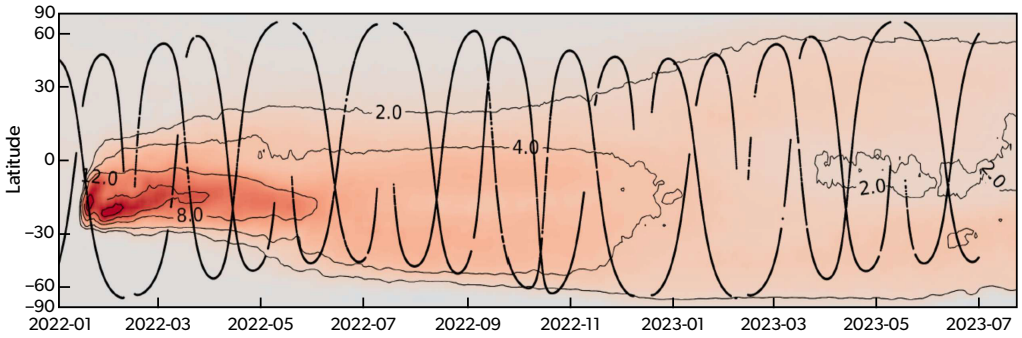

Figure S2.4: *SAGE III/ISS sampling locations overlaying the Hunga water vapour plume as observed by MLS, as a function of time and latitude. The MLS water vapour contours are the same as in Figure S2.1. Figure courtesy of Jon Starr at NSF NCAR.*

modelling assessments (Luo, 2016; Revell et al., 2017). For the Hunga HTHH-MOC experiments (Zhu et al., 2025), the CMIP6 methods from Luo (2016) were applied to generate SAD and waveband-mapped aerosol optical properties for the two years of the post-Hunga re-analysis experiment 2b (see Jörimann et al., 2025).

SSU stratospheric temperatures

Satellite data for studying long-term temperature changes in the middle and upper stratosphere include the operational Stratospheric Sounding Unit (SSU) covering 1979–2006 (Steiner et al., 2020). The SSU data represent broad-layer (approximately 15 km thick) averages centred around 30, 37, and 43 km. The SSU data originate from seven separate operational instruments, and a merged climate data record was developed by Zou et al. (2014), taking account of instrument calibration, satellite orbit drifts, and evolving CO_2 concentration.

The SSU data record beyond 2006 was extended by Zou and Qian (2016) using Advanced Microwave Sounding Unit (AMSU) measurements (the so-called SSU+AMSU data). MLS temperatures were used in Randel et al. (2016) to create an independent update to the SSU time series beyond 2006, based on constructing vertically weighted MLS averages to optimally match SSU for the overlap period 2004–2006 (the so-called SSU+MLS data).

SABER temperatures

The Sounding of the Atmosphere using Broadband Emission Radiometry (SABER) instrument on the Thermosphere, Ionosphere, Mesosphere Energetics and Dynamics (TIMED) satellite has measured temperature and chemical species in the middle atmosphere since January 2002 (Russell et al., 1999). Temperatures are retrieved from measurements of infrared CO_2 emissions from the atmospheric limb over altitudes from approximately 16 to 100 km, with a vertical resolution of 2 km (Remsberg et al., 2008).

Data used here are from retrieval version v2.08, available online at `https://saber.gats-inc.com`. SABER temperature profiles are available at two local times each day, with measurements from 53° latitude in one hemisphere to 83° latitude in the other. The local times of the measurements shift gradually from one day to the next as the TIMED orbit precesses, and this sampling pattern flips approximately every 65 days. Further data analysis details are described in Yu et al. (2023).

TROPOMI SO_2

SO_2 column abundances have been measured by the Tropospheric Monitoring Instrument (TROPOMI) operating on ESA's Sentinel-5 Precursor (S5P) satellite since 2017 (Veefkind et al., 2012). The polar-orbiting S5P satellite enables daily temporal resolution for TROPOMI SO_2 measurements at the tropical latitudes of the Hunga eruption.

TROPOMI uses observations of backscattered UV radiation to retrieve vertical column densities (VCDs) of volcanic SO_2 and is capable of detecting VCDs of less than 1 Dobson Unit (DU; 1 DU = 2.69×10^{16} molecules cm^{-2}) in a single pixel (Li et al., 2017; Theys et al., 2017). TROPOMI provides a spatial resolution of 5.5 × 3.5 km, and the total uncertainty of the TROPOMI stratospheric SO_2 measurements is approximately 35 % (Carn et al., 2022).

Reanalysis meteorological and constituent data sets

An atmospheric reanalysis system consists of a global forecast model, input observations, and a data assimilation scheme used in combination to produce

best estimates (gridded analyses) of past atmospheric states—including temperature, wind, geopotential height, and other meteorological fields.

An overview and description of atmospheric reanalysis systems, with a focus on the stratosphere, is provided by Fujiwara et al. (2017), and comprehensive evaluations of current reanalysis data in the stratosphere can be found in SPARC (2022). Stratospheric composition reanalysis is also available from the MERRA-2 Stratospheric Composition Reanalysis of Aura Microwave Limb Sounder (M2-SCREAM), which provides globally gridded analyses of the MLS constituents based on MERRA-2 winds (Wargan et al., 2023).

AIRS, IASI, CrIS temperatures, and airglow

There are several data sets used briefly in Chapter 6 regarding measurements of upper atmospheric waves observed after the initial Hunga eruption. These individual data sets are not described in detail in this Supplement, but further information can be found in Wright et al. (2022).

S2.2 Ground-based and balloon measurements

AERONET particle size distribution

The AErosol RObotic NETwork (AERONET) project (Holben et al., 1998; Zhang et al., 2006) was established to provide a harmonised network of ground-based sun photometers. AERONET observations are used to derive column-integrated aerosol parameters (Dubovik and King, 2000) and for satellite validation (e.g., Kahn et al., 2005; Remer and Kaufman, 2006), and contribute to a quantitative understanding of aerosol radiative effects (Kinne et al., 2003; Schulz et al., 2006).

The automatic Sun-tracking and sky-scanning radiometers make measurements every 15 minutes across multiple wavelengths (340, 380, 440, 500, 675, 870, 940, and 1020 nm). The detailed spectral information enables the derivation of a column particle size distribution (King et al., 1978; Eck et al., 1999). For example, Holben et al. (1996) demonstrated how measurements in the Amazon Basin during 1993 revealed a change in aerosol size distribution, transitioning from a background distribution (with modest Pinatubo enhancement) into a clear signature of biomass-burning aerosol during the dry season.

For the analysis of the Hunga aerosol size distribution in this report, the cloud-screened Level 1.5 observations are used, applying version 3 of the spectral inversion algorithm (Dubovik et al., 2006; Boichu et al., 2023).

COBALD backscatter sonde

The COBALD (Compact Optical Backscatter Aerosol Detector) instrument is a lightweight backscatter sonde designed to be flown on operational weather balloons. COBALD provides high-precision *in situ* measurements of aerosol backscatter coefficient at two wavelengths (455 and 940 nm), and detects backscattered light from air molecules, aerosol, or cloud droplets. These measurements provide detailed information on aerosol (or cloud) particle size and number density.

Ground-based GNSS Total Electron Content (TEC)

Ground-based networks of thousands of geodetic Global Navigation Satellite System (GNSS) receivers measure the phase advance and group delay on two or more frequencies, which can be used to estimate the path-integrated electron density of the ionosphere between transmitter and receiver satellites—referred to as the Total Electron Content (TEC) (Themens et al., 2013; Rideout and Coster, 2006).

This TEC is, by a wide margin, the most abundant ionospheric measurement available. While it can be subject to limitations from receiver and satellite bias calculation, for studies of the Hunga event and other mesoscale ionospheric structuring, relative TEC—where detrending has been applied—is generally accurate, albeit subject to some limitations depending on the signal ray geometry with respect to the orientation of the phase fronts of wave structures (Guerra et al., 2024).

Without projection to vertical, TEC can be determined with a precision as high as 0.005–0.02 TECU, depending on the phase stability of the receiver.

Ground-based lidar: aerosol extinction and scattering ratios

Réunion Island lidars (Maïdo observatory) A lidar facility has operated at Réunion Island (21°S, 55°E) since 1994 (Baray et al., 2013). Originally located at the coastal Université de La Réunion site in Saint-Denis (80 m a.s.l.), the system was relocated in 2012 to the Maïdo mountain observatory (2160 m a.s.l.).

The original Rayleigh–Mie 532 nm Nd:YAG lidar was upgraded in 1998 to a DIAL system to enable measurements of tropospheric ozone profiles (Baray et al., 1999). It was further adapted in 2002, incorporating Raman channels providing measurements

of water vapour profiles (Baray et al., 2013). A second aerosol-measuring DIAL lidar has been operational at Maïdo since June 2000.

As part of the NOAA Tonga Rapid Response Experiment (TR^2Ex), Baron et al. (2023) analysed the initial detections of the sheared Hunga aerosol layers, comparing results from both systems. They reported, among other findings, somewhat different lidar ratio (extinction-to-backscatter ratio) measurements between the two systems.

Lauder lidar The Lauder Atmospheric Research Station of the National Institute of Water and Atmospheric Research (NIWA), located on the South Island of New Zealand (45.0°S, 169.7°E, 370 m a.s.l.), has been operating a lidar at 532 nm since 1992 on a regular basis, with a mean measurement rate of one or two nights per week.

It provides measurements of both scattering ratio and particle depolarisation ratio. To retrieve vertical profiles of scattering ratio, a Fernald inversion method is used, assuming an aerosol extinction-to-backscatter ratio of 46 sr. The molecular backscattering coefficient is derived from the JRA-55 meteorological analysis (Nagai et al., 2010; Sakai et al., 2016).

Dumont d'Urville lidar The French Antarctic station Dumont d'Urville (66.6°S, 140°E; DDU) has hosted an aerosol and cloud lidar since April 1989, operating in the Network for the Detection of Atmospheric Composition Changes (NDACC). The main focus of the instrument is the study of polar stratospheric clouds with nighttime setup; the recent focus on aerosol plumes originating from either volcanic or biomass burning activity extended the measurement calendar to the summertime.

The Nd:YAG laser source emits at 532 nm at 10 Hz frequency with an emitted power of approximately 250 mJ. Backscattered photons are collected on a collocated 80 cm diameter Newton telescope. A polarising cube at the reception splits the beam into two components polarised parallel and perpendicular to the laser emission for the 532 nm wavelength, each component is recorded and inverted to calculate the depolarisation ratio. The Rayleigh/Mie/Raman lidar also acquires the N_2 vibrational Raman scattering at 607 nm. As the OHP lidar, the signal inversion is performed using the Klett-Fernald formalism derive scattering ratio profiles, which have a 60 m vertical resolution. ECMWF meteorological data is also used for the molecular backscattering calculation. A detailed description of the instrument, measurements processing method as well as error estimation is provided by Tencé et al. (2022).

Mauna Loa Lidar The NOAA Mauna Loa Observatory (19.5°N, 155.6°W, 3396 m a.s.l.) established a ruby laser-based lidar in the early 1970s, which operated until 1998. A Nd:YAG laser-based lidar began operation in 1994. The YAG system operates about once per week and retrieves aerosol profiles at 532 and 1064 nm at 300 m altitude resolution. Molecular profiles needed for analysis are calculated from radiosondes launched at Hilo, HI (56 km distant) and the NASA/MSIS model for altitudes above the radiosonde. The signal is usually normalised between 38 and 40 km and the Fernald-Klett inversion method is used (Barnes and Hofmann, 1997).

OHP lidar The Observatoire de Haute-Provence (OHP) located in southern France (43.9° N, 5.7° E, 670 m a.s.l.) is equipped with several lidar systems for atmospheric sounding at a wide range of altitudes. The aerosol measurements are provided by LTA lidar operating at 532 nm since 1991 on a regular basis with a mean measurement rate of 10-12 acquisition nights per month. For retrieving vertical profiles of stratospheric aerosol, a Fernald-Klett inversion method is used to provide backscatter and extinction coefficients. The scattering ratio is then computed as a ratio of total (molecular plus aerosol) to molecular backscattering, where the latter is derived from ECMWF meteorological analysis. The resulting vertical profiles of aerosol parameters are reported at 150 m vertical resolution. A more detailed description of the instruments, aerosol retrieval and error budget are provided by Khaykin et al. (2017) and references therein.

São Paulo (SPU) and Bauru (IPMET) lidars The lidar facility at São Paulo (SPU) is a multi-channel lidar system with elastic channels at 356, 532, and 1064 nm, and Raman channels at 530, 387, 408, and 530 nm (see, e.g., `https://www.spulidarstation.org/instruments`). Thanks in part to the cooperation and sharing of Hunga measurement data via the VolRes mailing list (e.g., Vernier et al., 2022; Vernier et al., 2024), a field campaign named *BraVo* took place in 2022 (Vernier et al., 2023). The campaign included lidar and balloon measurements from July to August to characterise and understand the progression of tropical Hunga aerosol and water vapour (Landulfo

et al., 2022b; Souza et al., 2025).

For the BraVo campaign, in addition to 13 balloon flights carried out (from May 24, 2022, to August 13, 2023), progression of the Hunga aerosol was monitored from the lidar facility at the Centro de Meteorologia de Bauru (IPMET-UNESP) in Bauru, Brazil (22.3°S, 49.3° W). The four-channel IPMET lidar measures at 355, 532, and 1064 nm, with the 532 nm channel measuring both parallel and perpendicular components used to derive depolarisation ratio for indicating non-spherical particles (Landulfo et al., 2022a).

Ionosonde electron density profiles

Ionosondes are ionospheric sounding instruments that use reflection in the high-frequency (HF) band (typically 1–25 MHz) to remotely sense the profile of ionospheric electron density up to the F2 peak of the ionosphere (Reinisch, 1987). These instruments have data records extending back to as early as 1932 and make up the majority of the ionospheric climate record. While these instruments are very reliable, automated processing of the radar data is challenging and often suffers critical errors during disturbed events that are not well characterised by the available quality control measures supplied with the automatically processed products (Stankov et al., 2023; Themens et al., 2022). Because of this limitation it is essential that the data from these instruments be manually processed during severe events, such as Hunga. When following the International Union of Radio Science (URSI)'s guidelines for data scaling and annotation, manually processed ionospheric peak critical frequency (f_oF2) can be taken, at the highest confidence level, as accurate to within 0.05 MHz, while h_mF2 can achieve a precision of between 5 km and 15 km, depending on ionospheric conditions and the competency of the manual scaler.

LOAC particle counter

The Light Optical Aerosol Counter (LOAC) is an optical particle counter instrument that can be operated on weather balloons for observations in the stratosphere (Renard et al., 2016). LOAC measures the number of aerosol particles at different particle sizes and additionally derives information about the absorption of the aerosol from two detectors (photodiodes) at two different angles from the light source (12 and 60 degrees). This design of the LOAC instrument allows calculation of a "particle typology" classification (Renard et al., 2016) based on the number of particles present and their light-absorbing properties.

In addition to the initial Réunion Island campaign (Kloss et al., 2022), the later Hunga aerosol was also profiled with the LOAC from South Africa in September 2022 (Cummins et al., 2023), and from Chile during 2023.

Lightweight aerosol filter samplers

A series of balloon soundings from São Paulo, Brazil deployed a lightweight filter sampling instrument to sample in-situ the composition of the Hunga aerosol. As part of the BraVo field campaign (Landulfo et al., 2022b), two phases of the campaign saw dedicated balloon soundings combining the filter sampler and POPC instrument to analyse the Hunga aerosol.

An initial series of soundings in May 2022 (Vernier et al., 2023), later soundings in August 2022 having a longer duration of sampling the Hunga aerosol (Vernier et al., 2024; Vernier et al., 2025), with the use of a radio-controlled device able to remain at a constant altitude to sample volcanic layers (personal communication Hazel Vernier, Dec 2023). The ion chromatography analysis for the samples from these two phases was carried out in two different laboratories (personal communication H. Vernier, December 2023), and the two instruments also differed in their detection limits.

For the August 2022 soundings analysed by Vernier et al. (2025), polytetrafluoroethene (PTFE) filters with a pore size of 0.45 µm were used. A key uncertainty remains regarding the collection efficiency of the finest particles, as to whether the sampler may have been unable to capture the smaller volcanic sulfate particles.

Ozonesondes and SO_2 sondes

Ozonesondes are small, lightweight, and compact balloon-borne instruments developed for measuring the vertical distribution of atmospheric ozone up to an altitude of about 30 km. Data used here are from the Electrochemical Concentration Cell (ECC) Ozonesonde, which provides ozone profile observations with an uncertainty of 10% (Tarasick et al., 2021). These measurements have a high vertical resolution of 5 m. The SO_2 sonde provides SO_2 profile measurements based on modification of an ECC ozonesonde, as described in Yoon et al. (2022). SO_2 measurements have an uncertainty of 20%.

POPS optical particle spectrometer

The Portable Optical Particle Spectrometer (POPS) is a lightweight, low-power, and relatively low-cost

research-grade optical particle counter that measures the number concentration of aerosol particles with diameters between 140 nm and 2.5 μm (Gao et al., 2016).

Since 2020, a global network of POPS launches has been established under the Balloon Baseline Stratospheric Aerosol Project (B^2SAP; e.g., Todt et al., 2023; Asher et al., 2024). Quarterly launches were conducted during 2022 from both the northern and southern tropics (Hilo, Hawaii, and Maïdo, Réunion Island, respectively) and from both northern and southern mid-latitudes (Boulder, USA, and Lauder, New Zealand).

Asher et al. (2023) use these data to study particle size variations within the Hunga volcanic cloud.

POPC Particle Counter

The BraVo balloon soundings used a POPC particle counter, a commercially available OPC instrument (Particle Plus 8306) that measures aerosol concentrations within 8 size channels, between 0.15 and 5 microns (Vernier et al., 2025).

The newer NPOPC, used on some flights, is an improved POPC instrument (Particle Plus, with similar laser, but improved signal-processing to provide 30 size channels). The POPC was also used in the DCOTSS field campaign, involving soundings from Kansas in August 2021 measuring volcanic aerosol from the La Soufrière eruption (Li et al., 2023).

STAC and L-OPC particle counters

The longest record of in-situ measurements of the stratospheric aerosol layer is from the continuing program of balloon soundings begun from Laramie, Wyoming in 1971 (Deshler et al., 2003; Deshler et al., 2019). The main basis of this record is the optical particle counter (OPC), measuring the number of scattering pulses of white light, corresponding to particles larger than approximately 300 nm diameter.

Since 2016, the Laramie record has continued with a smaller lighter-weight LASP OPC (LOPC, Kalnajs and Deshler, 2022), superseding the OPC40 that provided the Wyoming record since the late 1980s (Deshler et al., 2003). The earlier record used a similar 25 degree scattering OPC (Pinnick and Hofmann, 1973), also measuring from Minneapolis back to August 1963, originally known as a "dust-sonde" (Rosen, 1964).

In addition to the OPC, the Wyoming system also measures total particle number concentration using a condensation particle counter (CPC), counting ultrafine particles down to 10nm diameter. Now known as the Stratospheric Total Aerosol Counter (STAC; Deshler et al., 2024; Norgren et al., 2024), the instrument grows ultrafine particles to optically active sizes within a growth chamber (Rosen and Hofmann, 1977).

Soundings with the LOPC and STAC from McMurdo in 2019 and 2023 (Deshler et al., 2024) measured the long-range transport of the Hunga aerosol in April to June 2023. The LOPC has multiple size cuts, up to super-micron sizes, measuring also the size distribution of polar stratospheric clouds (Rosen et al., 1988; Deshler et al., 1994).

Radiosonde water vapour

Data from the operational upper-air network using the Vaisala RS41 radiosonde provide *in situ* observations of the large amounts of water vapour injected into the stratosphere by the Hunga eruption and allow a description of the early development of the volcanic plume as it dispersed.

Details regarding the Vaisala RS41 radiosonde observations here follows Vömel et al. (2022). The Vaisala RS41 humidity sensor relies on an integrated temperature sensor, which measures the sensor temperature in addition to air temperature, and the sensor temperature is used to eliminate any solar radiation dry bias. Furthermore, the sensor is heated to reduce icing and contamination. This allows direct exposure of the sensor to the atmosphere without any protective cap, which would otherwise reduce the ventilation around the sensor and allow for other artifacts. The Vaisala processing algorithm corrects the measured relative humidity (RH) for the difference between sensor and ambient temperature. The response time of the RS41 sensor increases strongly with decreasing temperature, reaching more than one minute at temperatures below −60 °C. The Vaisala algorithm compensates for the slow sensor response in addition to the correction due the elevated sensor temperature. The estimated detection limit of enhanced stratospheric water vapour based on these data lies around 100 ppmv at 30 km, 50 ppmv at 28 km and 15 ppmv at 25 km. Based on experience with tropospheric observations and extensive comparisons with other measurements, relative uncertainty values are in the range of 2 to 5% of the measured value. The vertical resolution of the measurements is better than 100 m.

References

Adriani, A., P. Massoli, G. Di Donfrancesco, F. Cairo, M. L. Moriconi and M. Snels (2004). 'Climatology of polar stratospheric clouds based on lidar observations from 1993 to 2001 over McMurdo Station, Antarctica'. *J. Geophys. Res.*, 109. DOI: 10.1029/2004jd004800.

Antuña-Marrero, J.-C., G. W. Mann, J. Barnes, A. Rodríguez-Vega, S. Shallcross, S. S. Dhomse, G. Fiocco and G. W. Grams (2021). 'Recovery of the first ever multi-year lidar dataset of the stratospheric aerosol layer, from Lexington, MA, and Fairbanks, AK, January 1964 to July 1965'. *Earth Syst. Sci. Data*, 13, pp. 4407–4423. DOI: 10.5194/essd-13-4407-2021.

Asher, E., A. Baron, P. Yu, M. Todt, P. Smale, B. Liley, R. Querel, T. Sakai, I. Morino, Y. Jin et al. (2024). 'Balloon Baseline Stratospheric Aerosol Profiles (B2SAP)—Perturbations in the Southern Hemisphere, 2019–2022'. *J. Geophys. Res.*, 129, e2024JD041581. DOI: 10.1029/2024jd041581.

Asher, E., M. Todt, K. Rosenlof, T. Thornberry, R.-S. Gao, G. Taha, P. Walter, S. Alvarez, J. Flynn, S. M. Davis et al. (2023). 'Unexpectedly rapid aerosol formation in the Hunga Tonga plume'. *Proc. Natl. Acad. Sci.*, 120, e2219547120. DOI: 10.1073/pnas.2219547120.

Baray, J.-L., Y. Courcoux, P. Keckhut, T. Portafaix, P. Tulet, J.-P. Cammas, A. Hauchecorne, S. Godin Beekmann, M. De Mazière, C. Hermans et al. (2013). 'Maïdo observatory: a new high-altitude station facility at Reunion Island (21° S, 55° E) for long-term atmospheric remote sensing and in situ measurements'. *Atmos. Meas. Tech.*, 6, pp. 2865–2877. DOI: 10.5194/amt-6-2865-2013.

Baray, J.-L., J. Leveau, J. Porteneuve, G. Ancellet, P. Keckhut, F. Posny and S. Baldy (1999). 'Description and evaluation of a tropospheric ozone lidar implemented on an existing lidar in the southern subtropics'. *Appl. Optics*, 38, 6808. DOI: 10.1364/ao.38.006808.

Barnes, J. E. and D. J. Hofmann (1997). 'Lidar measurements of stratospheric aerosol over Mauna Loa Observatory'. *Geophys. Res. Lett.*, 24, pp. 1923–1926. DOI: 10.1029/97GL01943.

Baron, A., P. Chazette, S. Khaykin, G. Payen, N. Marquestaut, N. Bègue and V. Duflot (2023). 'Early Evolution of the Stratospheric Aerosol Plume Following the 2022 Hunga Tonga-Hunga Ha'apai Eruption: Lidar Observations From Reunion (21°S, 55°E)'. *Geophys. Res. Lett.*, 50, e2022GL101751. DOI: 10.1029/2022gl101751.

Bernath, P. (2017). 'The Atmospheric Chemistry Experiment (ACE)'. *J. Quant. Spectrosc. Radiat. Transfer*, 186, pp. 3–16. DOI: 10.1016/j.jqsrt.2016.04.006.

Boichu, M., R. Grandin, L. Blarel, B. Torres, Y. Derimian, P. Goloub, C. Brogniez, I. Chiapello, O. Dubovik, T. Mathurin et al. (2023). 'Growth and Global Persistence of Stratospheric Sulfate Aerosols From the 2022 Hunga Tonga–Hunga Ha'apai Volcanic Eruption'. *J. Geophys. Res.*, 128, e2023JD039010. DOI: 10.1029/2023JD039010.

Boone, C. D., P. F. Bernath and M. Lecours (2023). 'Version 5 retrievals for ACE-FTS and ACE-imagers'. *J. Quant. Spectrosc. Radiat. Transfer*, 310, 108749. DOI: 10.1016/j.jqsrt.2023.108749.

Bourassa, A. E., D. A. Degenstein, R. L. Gattinger and E. J. Llewellyn (2007). 'Stratospheric aerosol retrieval with optical spectrograph and infrared imaging system limb scatter measurements'. *J. Geophys. Res.*, 112, D10217. DOI: 10.1029/2006JD008079.

Bourassa, A. E., D. J. Zawada, L. A. Rieger, T. W. Warnock, M. Toohey and D. A. Degenstein (2023). 'Tomographic retrievals of Hunga Tonga-Hunga Ha'apai volcanic aerosol'. *Geophys. Res. Lett.*, 50, e2022GL101978. DOI: 10.1029/2022GL101978.

Carn, S. A., N. A. Krotkov, B. L. Fisher and C. Li (2022). 'Out of the blue: volcanic SO_2 emissions during the 2021-2022 Hunga Tonga-Hunga Ha'apai eruptions'. *Front. Earth Sci.*, 13. DOI: 10.3389/feart.2022.976962.

Carslaw, K. S., B. Luo and T. Peter (1995). 'An analytic expression for the composition of aqueous HNO_3–H_2SO_4 stratospheric aerosols including gas phase removal of HNO_3'. *Geophys. Res. Lett.*, 22, pp. 1877–1880. DOI: 10.1029/95GL01668.

Carslaw, K. S., B. P. Luo, S. L. Clegg, T. Peter, P. Brimblecombe and P. J. Crutzen (1994). 'Stratospheric aerosol growth and HNO3 gas phase depletion from coupled HNO3 and water uptake by liquid particles'. *Geophys. Res. Lett.*, 21, pp. 2479–2482. DOI: 10.1029/94gl02799.

Chen, Z., P. K. Bhartia, R. Loughman, P. Colarco and M. DeLand (2018). 'Improvement of stratospheric aerosol extinction retrieval from OMPS/LP using a new aerosol model'. *Atmos. Meas. Tech.*, 11, pp. 6495–6509. DOI: 10.5194/amt-11-6495-2018.

Clerbaux, C., A. Boynard, L. Clarisse, M. George, J. Hadji-Lazaro, H. Herbin, D. Hurtmans, M. Pommier,

A. Razavi, S. Turquety et al. (2009). 'Monitoring of atmospheric composition using the thermal infrared IASI/MetOp sounder'. *Atmos. Chem. Phys.*, 9, pp. 6041–6054. DOI: 10.5194/acp-9-6041-2009.

Cummins, D. P., V. Guemas, C. J. Cox, M. R. Gallagher and M. D. Shupe (2023). 'Surface Turbulent Fluxes From the MOSAiC Campaign Predicted by Machine Learning'. *Geophys. Res. Lett.*, 50, e2023GL105698. DOI: 10.1029/2023GL105698.

Currie, J. L., B. A. Carter, T. Dao and M. Terkildsen (2021). 'The importance of counting: A new index to correctly quantify Equatorial Plasma Bubble occurrence in COSMIC Radio Occultation data'. *J. Geophys. Res.*, 126, e2021JA029539. DOI: 10.1029/2021JA029539.

Damadeo, R. P., J. M. Zawodny, L. W. Thomason and N. Iyer (2013). 'SAGE v7.0 algorithm: Application to SAGE II'. *Atmos. Meas. Tech.*, 6, pp. 3539–3561. DOI: 10.5194/amt-6-3539-2013.

Davis, S. M., R. Damadeo, D. Flittner, K. H. Rosenlof, M. Park, W. J. Randel et al. (2021). 'Validation of SAGE III/ISS solar water vapor data with correlative satellite and balloon-borne measurements'. *J. Geophys. Res.*, 125, e2020JD033803. DOI: 10.1029/2020JD033803.

Degenstein, D. A., E. J. Llewellyn and N. D. Lloyd (2003). 'Volume emission rate tomography from a satellite platform'. *Appl. Optics*, 42, pp. 1441–1450. DOI: 10.1364/AO.42.001441.

Deshler, T., M. E. Hervig, D. J. Hofmann, J. M. Rosen and J. B. Liley (2003). 'Thirty years of in situ stratospheric aerosol size distribution measurements from Laramie, Wyoming (41°N), using balloon-borne instruments'. *J. Geophys. Res.*, 108. DOI: 10.1029/2002JD002514.

Deshler, T., B. Luo, M. Kovilakam, T. Peter and L. E. Kalnajs (2019). 'Retrieval of aerosol size distributions from in situ particle counter measurements: Instrument counting efficiency and comparisons with satellite measurements'. *J. Geophys. Res.*, 124, pp. 5058–5087. DOI: 10.1029/2018JD029558.

Deshler, T., B. J. Johnson and W. R. Rozier (1994). 'Changes in the Character of Polar Stratospheric Clouds Over Antarctica in 1992 Due to the Pinatubo Volcanic Aerosol'. *Geophys. Res. Lett.*, 21, pp. 273–276. DOI: 10.1029/94GL00072.

Deshler, T., L. E. Kalnajs, M. Norgren, Y. Zhu and J. Zhang (2024). 'In Situ Aerosol Size Spectra Measurements in the Austral Polar Vortex Before and After the Hunga Tonga-Hunga Ha'apai Volcanic Eruption'. *Geophys. Res. Lett.*, 51, e2024GL111388. DOI: 10.1029/2024gl111388.

Dhomse, S. S., G. W. Mann, J. C. Antuña Marrero, S. E. Shallcross, M. P. Chipperfield, K. S. Carslaw, L. Marshall, N. L. Abraham and C. E. Johnson (2020). 'Evaluating the simulated radiative forcings, aerosol properties, and stratospheric warmings from the 1963 Mt Agung, 1982 El Chichón, and 1991 Mt Pinatubo volcanic aerosol clouds'. *Atmos. Chem. Phys.*, 20, pp. 13627–13654. DOI: 10.5194/acp-20-13627-2020.

Dubovik, O. and M. D. King (2000). 'A flexible inversion algorithm for retrieval of aerosol optical properties from Sun and sky radiance measurements'. *J. Geophys. Res.*, 105, pp. 20673–20696. DOI: 10.1029/2000JD900282.

Dubovik, O., A. Sinyuk, T. Lapyonok, B. N. Holben, M. Mishchenko, P. Yang, T. F. Eck, H. Volten, O. Muñoz, B. Veihelmann et al. (2006). 'Application of spheroid models to account for aerosol particle nonsphericity in remote sensing of desert dust'. *J. Geophys. Res.*, 111. DOI: 10.1029/2005JD006619.

Duchamp, C., F. Wrana, B. Legras, P. Sellitto, R. Belhadji and C. von Savigny (2023). 'Observation of the aerosol plume from the 2022 Hunga Tonga–Hunga Ha'apai eruption with SAGE III/ISS'. *Geophys. Res. Lett.*, 50, e2023GL105076. DOI: 10.1029/2023GL105076.

Eck, T. F., B. N. Holben, J. S. Reid, O. Dubovik, A. Smirnov, N. T. O'Neill, I. Slutsker and S. Kinne (1999). 'Wavelength dependence of the optical depth of biomass burning, urban, and desert dust aerosols'. *J. Geophys. Res.*, 104, pp. 31333–31349. DOI: 10.1029/1999JD900923.

Eyring, V., S. Bony, G. A. Meehl, C. A. Senior, B. Stevens, R. J. Stouffer and K. E. Taylor (2016). 'Overview of the Coupled Model Intercomparison Project Phase 6 (CMIP6) experimental design and organization'. *Geosci. Model Dev.*, 9, pp. 1937–1958. DOI: 10.5194/gmd-9-1937-2016.

Eyring, V., N. R. P. Harris, M. Rex, T. G. Shepherd, D. W. Fahey, G. T. Amanatidis, J. Austin, M. P. Chipperfield, M. Dameris, P. M. D. F. Forster et al. (2005). 'A Strategy for Process-Oriented Validation of Coupled Chemistry–Climate Models'. *Bull. Am. Meteorol. Soc.*, 86, pp. 1117–1134. DOI: 10.1175/bams-86-8-1117.

Fujiwara, M., J. S. Wright, G. L. Manney, L. J. Gray, J. Anstey, T. Birner, S. Davis, E. P. Gerber, V. L. Harvey, M. I. Hegglin et al. (2017). 'Introduction to the SPARC Reanalysis Intercomparison Project

(S-RIP) and overview of the reanalysis systems'. *Atmos. Chem. Phys.*, 17, pp. 1417–1452. DOI: 10.5194/acp-17-1417-2017.

Gao, R. S., H. Telg, R. J. McLaughlin, S. J. Ciciora, L. A. Watts, M. S. Richardson, J. P. Schwarz, A. E. Perring, T. D. Thornberry, A. W. Rollins et al. (2016). 'A lightweight, high-sensitivity particle spectrometer for PM2.5 aerosol measurements'. *Aerosol Sci. Technol.*, 50, pp. 88–99. DOI: 10.1080/02786826.2015.1131809.

Gelaro, R., W. McCarty, M. J. Suárez, R. Todling, A. Molod, L. Takacs, C. A. Randles, A. Darmenov, M. G. Bosilovich and R. Reichle (2017). 'The Modern-Era Retrospective Analysis for Research and Applications, Version 2 (MERRA-2)'. *J. Climate*, 30, pp. 5419–5454. DOI: 10.1175/jcli-d-16-0758.1.

Guerra, M., C. Cesaroni, M. Ravanelli and L. Spogli (2024). 'Travelling ionospheric disturbances detection: A statistical study of detrending techniques, induced period error and near real-time observables'. *J. Space Weather Space Clim.*, 14. DOI: 10.1051/swsc/2024017.

Holben, B. N., T. F. Eck, I. Slutsker, D. Tanré, J. P. Buis, A. Setzer, E. Vermote, J. A. Reagan, Y. J. Kaufman, T. Nakajima et al. (1998). 'AERONET—A Federated Instrument Network and Data Archive for Aerosol Characterization'. *Remote Sens. Environ.*, 66, pp. 1–16. DOI: 10.1016/S0034-4257(98)00031-5.

Holben, B. N., A. Setzer, T. F. Eck, A. Pereira and I. Slutsker (1996). 'Effect of dry-season biomass burning on Amazon basin aerosol concentrations and optical properties, 1992–1994'. *J. Geophys. Res.*, 101, pp. 19465–19481. DOI: 10.1029/96JD01114.

Hurst, D. F., W. G. Read, H. Vömel, H. B. Selkirk, K. H. Rosenlof, S. M. Davis, E. G. Hall, A. F. Jordan and S. J. Oltmans (2016). 'Recent divergences in stratospheric water vapor measurements by frost point hygrometers and the Aura Microwave Limb Sounder'. *Atmos. Meas. Tech.*, 9, pp. 4447–4457. DOI: 10.5194/amt-9-4447-2016.

Jäger, H. and T. Deshler (2002). 'Lidar backscatter to extinction, mass and area conversions for stratospheric aerosols based on midlatitude balloonborne size distribution measurements'. *Geophys. Res. Lett.*, 29. DOI: 10.1029/2002gl015609.

Jörimann, A., T. Sukhodolov, B. Luo, G. Chiodo, G. Mann and T. Peter (2025). 'REtrieval Method for optical and physical Aerosol Properties in the stratosphere (REMAPv1)'. *Geosci. Model Dev.*, 18, pp. 6023–6041. DOI: 10.5194/gmd-18-6023-2025.

Kahn, R. A. and B. J. Gaitley (2015). 'An analysis of global aerosol type as retrieved by MISR'. *J. Geophys. Res.*, 120, pp. 4248–4281. DOI: 10.1002/2015JD023322.

Kahn, R. A., B. J. Gaitley, M. J. Garay, D. J. Diner, T. F. Eck, A. Smirnov and B. N. Holben (2010). 'Multiangle Imaging Spectroradiometer global aerosol product assessment by comparison with the Aerosol Robotic Network'. *J. Geophys. Res.*, 115, D23209. DOI: 10.1029/2010JD014601.

Kahn, R. A., B. J. Gaitley, J. V. Martonchik, D. J. Diner, K. A. Crean and B. N. Holben (2005). 'Multiangle Imaging Spectroradiometer (MISR) global aerosol optical depth validation based on two years of coincident AERONET observations'. *J. Geophys. Res.*, 110, D10S04. DOI: 10.1029/2004JD004706.

Kahn, R. A., J. A. Limbacher, K. T. Junghenn Noyes, V. J. B. Flower, L. M. Zamora and K. F. McKee (2024). 'Evolving Particles in the 2022 Hunga Tonga—Hunga Ha'apai Volcano Eruption Plume'. *J. Geophys. Res.*, 129, e2023JD039963. DOI: 10.1029/2023JD039963.

Kalnajs, L. E. and T. Deshler (2022). 'A New Instrument for Balloon-Borne In Situ Aerosol Size Distribution Measurements, the Continuation of a 50 Year Record of Stratospheric Aerosols Measurements'. *J. Geophys. Res.*, 127, e2022JD037485. DOI: 10.1029/2022JD037485.

Kar, J., K.-P. Lee, M. A. Vaughan, J. L. Tackett, C. R. Trepte, D. M. Winker, P. L. Lucker and B. J. Getzewich (2019). 'CALIPSO level 3 stratospheric aerosol profile product: version 1.00 algorithm description and initial assessment'. *Atmos. Meas. Tech.*, 12, pp. 6173–6191. DOI: 10.5194/amt-12-6173-2019.

Khaykin, S. M., S. Godin-Beekmann, P. Keckhut, A. Hauchecorne, J. Jumelet, J.-P. Vernier, A. Bourassa, D. A. Degenstein, L. A. Rieger, C. Bingen et al. (2017). 'Variability and evolution of the midlatitude stratospheric aerosol budget from 22 years of ground-based lidar and satellite observations'. *Atmos. Chem. Phys.*, 17, pp. 1829–1845. DOI: 10.5194/acp-17-1829-2017.

Khaykin, S. M., S. Godin-Beekmann, A. Hauchecorne, J. Pelon, F. Ravetta and P. Keckhut (2018). 'Stratospheric smoke with unprecedentedly high backscatter observed by lidars above southern France'. *Geophys. Res. Lett.*, 45, pp. 1639–1646. DOI: 10.1002/2017GL076763.

Khaykin, S., A. Podglajen, F. Ploeger, J.-U. Grooß, F. Tence, S. Bekki, K. Khlopenkov, K. Bedka, L. Rieger, A. Baron et al. (2022). 'Global perturbation of stra-

tospheric water and aerosol burden by Hunga eruption'. *Commun. Earth Environ.*, 3, 316. DOI: 10.1038/s43247-022-00652-x.

Kim, M.-H., A. H. Omar, J. L. Tackett, M. A. Vaughan, D. M. Winker, C. R. Trepte, Y. Hu, Z. Liu, L. R. Poole, M. C. Pitts et al. (2018). 'The CALIPSO version 4 automated aerosol classification and lidar ratio selection algorithm'. *Atmos. Meas. Tech.*, 11, pp. 6107–6135. DOI: 10.5194/amt-11-6107-2018.

King, M. D., D. M. Byrne, B. M. Herman and J. A. Reagan (1978). 'Aerosol Size Distributions Obtained by Inversions of Spectral Optical Depth Measurements'. *J. Atmos. Sci.*, 35, pp. 2153–2167. DOI: 10.1175/1520-0469(1978)035<2153:ASDOBI>2.0.CO;2.

Kinne, S., U. Lohmann, J. Feichter, M. Schulz, C. Timmreck, S. Ghan, R. Easter, M. Chin, P. Ginoux, T. Takemura et al. (2003). 'Monthly averages of aerosol properties: A global comparison among models, satellite data, and AERONET ground data'. *J. Geophys. Res.*, 108, 4634. DOI: 10.1029/2001JD001253.

Kloss, C., P. Sellitto, J.-B. Renard, A. Baron, N. Bègue, B. Legras, G. Berthet, E. Briaud, E. Carboni, C. Duchamp et al. (2022). 'Aerosol characterization of the stratospheric plume from the volcanic eruption at Hunga Tonga 15 January 2022'. *Geophys. Res. Lett.*, 49, e2022GL099394. DOI: 10.1029/2022GL099394.

Knepp, T. N., M. Kovilakam, L. Thomason and S. J. Miller (2024). 'Characterization of stratospheric particle size distribution uncertainties using SAGE II and SAGE III/ISS extinction spectra'. *Atmos. Meas. Tech.*, 17, pp. 2025–2054. DOI: 10.5194/amt-17-2025-2024.

Kovilakam, M., L. W. Thomason, N. Ernest, L. Rieger, A. Bourassa and L. Millán (2020). 'The Global Space-based Stratospheric Aerosol Climatology (version 2.0): 1979–2018'. *Earth Syst. Sci. Data*, 12, pp. 2607–2634. DOI: 10.5194/essd-12-2607-2020.

Kovilakam, M., L. W. Thomason, M. Verkerk, T. Aubry and T. N. Knepp (2025). 'OMPS-LP aerosol extinction coefficients and their applicability in GloSSAC'. *Atmos. Chem. Phys.*, 25, pp. 535–553. DOI: 10.5194/acp-25-535-2025.

Landulfo, E., F. S. Lopes, J. C. Antuña, R. Arredondo and G. Taha (2022a). *Monitoring stratospheric aerosols in South America with ground-based lidar.* https://homepages.see.leeds.ac.uk/~amtgwm/SSirC_Landulfo_ForShareOffUnivLeedsSEEpage.pdf. May 2022 SSiRC workshop presentation.

Landulfo, E., F. S. Lopes, J.-P. Vernier, J. C. Antuña and the LALINET team (2022b). *VolRes and the BRAVO field campaign.* https://homepages.see.leeds.ac.uk/~amtgwm/SSirC_BRAVO_Landulfo_ForShareOffSEEpage.pdf. May 2022 SSiRC workshop presentation.

Legras, B., C. Duchamp, P. Sellitto, A. Podglajen, E. Carboni, R. Siddans, J.-U. Grooß, S. Khaykin and F. Ploeger (2022). 'The evolution and dynamics of the Hunga Tonga–Hunga Ha'apai sulfate aerosol plume in the stratosphere'. *Atmos. Chem. Phys.*, 22, pp. 14957–14970. DOI: 10.5194/acp-22-14957-2022.

Li, C., N. A. Krotkov, S. A. Carn, Y. Zhang, R. J. D. Spurr and J. Joiner (2017). 'New-generation NASA Aura Ozone Monitoring Instrument volcanic SO_2 dataset: Algorithm description, initial results, and continuation with the Suomi-NPP Ozone Mapping and Profiler Suite'. *Atmos. Meas. Tech.*, 10, pp. 445–458. DOI: 10.5194/amt-10-445-2017.

Li, Y., C. Pedersen, J. Dykema, J.-P. Vernier, S. Vattioni, A. K. Pandit, A. Stenke, E. Asher, T. Thornberry, M. A. Todt et al. (2023). 'In situ measurements of perturbations to stratospheric aerosol and modeled ozone and radiative impacts following the 2021 La Soufrière eruption'. *Atmos. Chem. Phys.*, 23, pp. 15351–15364. DOI: 10.5194/acp-23-15351-2023.

Limbacher, J. A., R. A. Kahn and J. Lee (2022). 'The new MISR research aerosol retrieval algorithm: A multi-angle, multi-spectral, bounded-variable least-squares retrieval of aerosol particle properties over both land and water'. *Atmos. Meas. Tech.*, 15, pp. 6865–6887. DOI: 10.5194/amt-15-6865-2022.

Livesey, N. J., W. G. Read, P. A. Wagner, L. Froidevaux, A. Lambert, G. L. Manney et al. (2020). *EOS MLS Version 4.2x Level 2 and 3 data quality and description document.* Technical Report JPL-D33509 Rev. E. https://mls.jpl.nasa.gov/data/v4-2_data_quality_document.pdf. Jet Propulsion Laboratory, California Institute of Technology.

Livesey, N. J., W. G. Read, P. A. Wagner, L. Froidevaux, M. L. Santee, M. J. Schwartz et al. (2022). *EOS MLS Version 5.0x Level 2 and 3 data quality and description document.* Technical Report JPL-D105336 Rev. B. https://mls.jpl.nasa.gov/data/v5-0_data_quality_document.pdf. Jet Propulsion Laboratory, California Institute of Technology.

Livesey, N. J., W. G. Read, L. Froidevaux, A. Lambert, M. L. Santee, M. J. Schwartz, L. F. Millán, R. F. Jarnot, P. A. Wagner, D. F. Hurst et al. (2021). 'Investigation and amelioration of long-term instrumental drifts in water vapor and nitrous oxide measurements

from the Aura Microwave Limb Sounder (MLS) and their implications for studies of variability and trends'. *Atmos. Chem. Phys.*, 21, pp. 15409–15430. DOI: 10.5194/acp-21-15409-2021.

Loughman, R. P., P. K. Bhartia, Z. Chen, P. Xu, E. Nyaku and G. Taha (2018). 'The Ozone Mapping and Profiler Suite (OMPS) Limb Profiler Version 1 aerosol extinction retrieval algorithm: Theoretical basis'. *Atmos. Meas. Tech.*, 11, pp. 2633–2651. DOI: 10.5194/amt-11-2633-2018.

Luo, B. (2016). *Stratospheric aerosol data for use in CMIP6 models*. ftp://iacftp.ethz.ch/pub_read/luo/CMIP6/Readme_Data_Description.pdf.

Millán, L., M. L. Santee, A. Lambert, N. J. Livesey, F. Werner, M. J. Schwartz, H. C. Pumphrey, G. L. Manney, Y. Wang, H. Su et al. (2022). 'The Hunga Tonga-Hunga Ha'apai Hydration of the Stratosphere'. *Geophys. Res. Lett.*, 49, e2022GL099381. DOI: 10.1029/2022gl099381.

Morgenstern, O., M. I. Hegglin, E. Rozanov, F. M. O'Connor, N. L. Abraham, H. Akiyoshi, A. T. Archibald, S. Bekki, N. Butchart, M. P. Chipperfield et al. (2017). 'Review of the global models used within phase 1 of the Chemistry–Climate Model Initiative (CCMI)'. *Geosci. Model Dev.*, 10, pp. 639–671. DOI: 10.5194/gmd-10-639-2017.

Nagai, T., B. Liley, T. Sakai, T. Shibata and O. Uchino (2010). 'Post-Pinatubo Evolution and Subsequent Trend of the Stratospheric Aerosol Layer Observed by Mid-Latitude Lidars in Both Hemispheres'. *Scientific Online Letters on the Atmosphere (SOLA)*, 6, pp. 69–72. DOI: 10.2151/sola.2010-018.

Norgren, M., L. E. Kalnajs and T. Deshler (2024). 'Measurements of Total Aerosol Concentration in the Stratosphere: A New Balloon-Borne Instrument and a Report on the Existing Measurement Record'. *J. Geophys. Res.*, 129, e2024JD040992. DOI: 10.1029/2024JD040992.

Park, M., W. J. Randel, R. P. Damadeo, D. E. Flittner, S. M. Davis, K. H. Rosenlof, N. Livesey, A. Lambert and W. Read (2021). 'Near-Global Variability of Stratospheric Water Vapor Observed by SAGE III/ISS'. *J. Geophys. Res.*, 126, e2020JD034274. DOI: 10.1029/2020JD034274.

Pedatella, N. M., X. Yue and W. S. Schreiner (2015). 'An improved inversion for FORMOSAT-3/COSMIC ionosphere electron density profiles'. *J. Geophys. Res.*, 120, pp. 8942–8953. DOI: 10.1002/2015JA021704.

Pinnick, R. G. and D. J. Hofmann (1973). 'Efficiency of light-scattering aerosol particle counters'. *Appl. Optics*, 12, pp. 2593–2597. DOI: 10.1364/AO.12.002593.

Pitts, M. C., L. R. Poole and R. Gonzalez (2018). 'Polar stratospheric cloud climatology based on CALIPSO spaceborne lidar measurements from 2006 to 2017'. *Atmos. Chem. Phys.*, 18, pp. 10881–10913. DOI: 10.5194/acp-18-10881-2018.

Prata, A. T., S. A. Young, S. T. Siems and M. J. Manton (2017). 'Lidar ratios of stratospheric volcanic ash and sulfate aerosols retrieved from CALIOP measurements'. *Atmos. Chem. Phys.*, 17, pp. 8599–8618. DOI: 10.5194/acp-17-8599-2017.

Randel, W. J., B. R. Johnston, J. J. Braun, S. Sokolovskiy, H. Vömel, A. Podglajen and B. Legras (2023). 'Stratospheric Water Vapor from the Hunga Tonga–Hunga Ha'apai Volcanic Eruption Deduced from COSMIC-2 Radio Occultation'. *Remote Sens.*, 15, 2167, p. 2167. DOI: 10.3390/rs15082167.

Randel, W. J., A. K. Smith, F. Wu, C.-Z. Zou and H. Qian (2016). 'Stratospheric Temperature Trends over 1979–2015 Derived from Combined SSU, MLS, and SABER Satellite Observations'. *J. Climate*, 29, pp. 4843–4859. DOI: 10.1175/jcli-d-15-0629.1.

Reinisch, B. W. (1987). 'New Techniques in Ground-Based Ionospheric Sounding and Studies'. *Radio Sci.*, 21, pp. 331–341. DOI: 10.1029/RS021i003p00331.

Remer, L. A. and Y. J. Kaufman (2006). 'Aerosol direct radiative effect at the top of the atmosphere over cloud free ocean derived from four years of MODIS data'. *Atmos. Chem. Phys.*, 6, pp. 237–253. DOI: 10.5194/acp-6-237-2006.

Remsberg, E. E., B. T. Marshall, M. Garcia-Comas, D. Krueger, G. S. Lingenfelser, J. Martin-Torres, M. G. Mlynczak, J. M. Russell III, A. K. Smith, Y. Zhao et al. (2008). 'Assessment of the quality of the Version 1.07 temperature-versus-pressure profiles of the middle atmosphere from TIMED/SABER'. *J. Geophys. Res.*, 113. DOI: 10.1029/2008JD010013.

Renard, J.-B., F. Dulac, G. Berthet, T. Lurton, D. Vignelles, F. Jégou, T. Tonnelier, M. Jeannot, B. Couté, R. Akiki et al. (2016). 'LOAC: a small aerosol optical counter/sizer for ground-based and balloon measurements of the size distribution and nature of atmospheric particles – Part 1: Principle of measurements and instrument evaluation'. *Atmos. Meas. Tech.*, 9, pp. 1721–1742. DOI: 10.5194/amt-9-1721-2016.

Revell, L. E., A. Stenke, B. Luo, S. Kremser, E. Rozanov, T. Sukhodolov and T. Peter (2017). 'Impacts of Mt Pinatubo volcanic aerosol on the tropical

stratosphere in chemistry–climate model simulations using CCMI and CMIP6 stratospheric aerosol data'. *Atmos. Chem. Phys.*, 17, pp. 13139–13150. DOI: 10.5194/acp-17-13139-2017.

Rideout, W. and A. Coster (2006). 'Automated GPS processing for global total electron content data'. *GPS Solutions*, 10, pp. 219–228. DOI: 10.1007/s10291-006-0029-5.

Rosen, J. M. (1964). 'The vertical distribution of dust to 30 km'. *J. Geophys. Res.*, 69, pp. 4673–4676. DOI: 10.1029/JZ069i021p04673.

Rosen, J. M. and D. J. Hofmann (1977). 'Balloon-borne measurements of condensation nuclei'. *J. Appl. Meteorol.*, 16, pp. 56–62. DOI: 10.1175/1520-0450(1977)016<0056:BMOCN>2.0.CO;2.

Rosen, J. M., D. J. Hofmann and J. W. Harder (1988). 'Aerosol measurements in the winter/spring Antarctic stratosphere. 2. Impact on Polar Stratospheric Cloud theories'. *J. Geophys. Res.*, 93, pp. 677–686. DOI: 10.1029/JD093iD01p00677.

Rozanov, A., C. Pohl, C. Arosio, A. Bourassa, K. Bramstedt, E. Malinina, L. Rieger and J. P. Burrows (2024). 'Retrieval of stratospheric aerosol extinction coefficients from sun-normalized Ozone Mapper and Profiler Suite Limb Profiler (OMPS-LP) measurements'. *Atmos. Meas. Tech.*, 17, pp. 6677–6695. DOI: 10.5194/amt-17-6677-2024.

Russell, J. M., M. G. Mlynczak, L. L. Gordley, J. Tansock and R. Esplin (1999). 'Overview of the SABER experiment and preliminary calibration results'. *SPIE Proc.*, 3756, pp. 277–288. DOI: 10.1117/12.366382.

Ryan, R. A., M. A. Vaughan, S. D. Rodier, J. L. Tackett, J. A. Reagan, R. A. Ferrare, J. W. Hair, J. A. Smith and B. J. Getzewich (2024). 'Total column optical depths retrieved from CALIPSO lidar ocean surface backscatter'. *Atmos. Meas. Tech.*, 17, pp. 6517–6545. DOI: 10.5194/amt-17-6517-2024.

Sakai, T., O. Uchino, T. Nagai, B. Liley, I. Morino and T. Fujimoto (2016). 'Long-term variation of stratospheric aerosols observed with lidars over Tsukuba, Japan, from 1982 and Lauder, New Zealand, from 1992 to 2015'. *J. Geophys. Res.*, 121, pp. 10, 283–10, 293. DOI: 10.1002/2016JD025132.

Saunders, R., J. Hocking, E. Turner, P. Rayer, M. Matricardi, A. Geer et al. (2018). 'An update on the RTTOV fast radiative transfer model (currently at version 12)'. *Geosci. Model Dev.*, 11, pp. 2717–2737. DOI: 10.5194/gmd-11-2717-2018.

Savigny, C. von and C. G. Hoffmann (2020). 'Issues related to the retrieval of stratospheric-aerosol particle size information based on optical measurements'. *Atmos. Meas. Tech.*, 13, pp. 1909–1920. DOI: 10.5194/amt-13-1909-2020.

Schulz, M., C. Textor, S. Kinne, Y. Balkanski, S. Bauer, T. Berntsen, T. Berglen, O. Boucher, F. Dentener, S. Guibert et al. (2006). 'Radiative forcing by aerosols as derived from the AeroCom present-day and pre-industrial simulations'. *Atmos. Chem. Phys.*, 6, pp. 5225–5246. DOI: 10.5194/acp-6-5225-2006.

Sellitto, P., H. Guermazi, E. Carboni, R. Siddans and M. Burton (2019). 'Unified quantitative observation of coexisting volcanic sulfur dioxide and sulfate aerosols using ground-based Fourier transform infrared spectroscopy'. *Atmos. Meas. Tech.*, 12, pp. 5381–5389. DOI: 10.5194/amt-12-5381-2019.

Sellitto, P., R. Siddans, R. Belhadji, E. Carboni, B. Legras, A. Podglajen and et al. (2024). 'Observing the SO_2 and sulfate aerosol plumes from the 2022 Hunga eruption with the Infrared Atmospheric Sounding Interferometer (IASI)'. *Geophys. Res. Lett.*, 51, e2023GL105565. DOI: 10.1029/2023GL105565.

Shaikh, M. M., R. Notarpietro and B. Nava (2014). 'The impact of spherical symmetry assumption on radio occultation data inversion in the ionosphere: An assessment study'. *Adv. Space Res.*, 53, pp. 599–608. DOI: 10.1016/j.asr.2013.10.025.

Shallcross, S. E. (2020). 'The role of volcanic ash in the global dispersion of the aerosol cloud from major tropical eruptions'. https://etheses.whiterose.ac.uk/id/eprint/28125/1/Sarah_Shallcross_PhD_thesis.pdf. PhD thesis. University of Leeds.

Siddans, R. (2019). *Water Vapour Climate Change Initiative (WV_cci) – Phase One, Deliverable 2.2; Version 1.0, 27 March 2019*. Technical Report. https://climate.esa.int/documents/1337/Water_Vapour_CCI_D2.2_ATBD_Part2-IMS_L2_product_v1.0.pdf. European Space Agency (ESA) / ECSAT.

Siddans, R. (2023). *Water Vapour Climate Change Initiative (WV_cci) – Phase Two, ATBD Part 2 – IMS L2 Product, Version 2.0, 21 November 2023*. Technical Report CCIWV.REP.005, D2.2. https://climate.esa.int/media/documents/Water_Vapour_CCI_D2.2_ATBD_Part2-IMS_L2_product_v2.0.pdf. European Space Agency (ESA) / ECSAT.

Souza, G., J.-P. Vernier, D. Quintão, B. Biazon, F. Lopes, J. Ricardo, A. K. Pandit, R. C. Das, H. Liu, T. N. N. Knepp et al. (2025). 'Sedimentation and growth of volcanic aerosols within the Hunga plume: Insights from unique tropical in situ and satellite measurements'. *ESS Open Archive*, DOI: 10.22541/essoar.174241613.36494891/v1.

SPARC (2006). *Assessment of Stratospheric Aerosol Properties (ASAP)*. Tech. rep. SPARC Report No. 4. https://www.aparc-climate.org/publications/sparc-reports/sparc-report-no-4/. Stratosphere–troposphere Processes and their Role in Climate (SPARC) Project, WCRP.

SPARC (2022). *Reanalysis Intercomparison Project (S-RIP) Final Report*. Tech. rep. SPARC Report No. 10, WCRP-6/2021. https://www.aparc-climate.org/sparc-reports/sparc-report-no-10/. SPARC/WCRP.

Stankov, S. M., T. G. W. Verhulst and D. Sapundjiev (2023). 'Automatic Ionospheric Weather Monitoring With DPS-4D Ionosonde and ARTIST-5 Autoscaler: System Performance at a Mid-Latitude Observatory'. *Radio Sci.*, 58, e2022RS007628. DOI: 10.1029/2022RS007628.

Steiner, A. K., F. Ladstädter, W. J. Randel, A. C. Maycock, Q. Fu, C. Claud, H. Gleisner, L. Haimberger, S.-P. Ho and P. Keckhut (2020). 'Observed temperature changes in the troposphere and stratosphere from 1979 to 2018'. *J. Climate*, 33, pp. 8165–8194. DOI: 10.1175/jcli-d-19-0998.1.

Stephens, G. L., D. G. Vane, R. J. Boain, G. G. Mace, K. Sassen, Z. Wang, A. J. Illingworth, E. J. O'connor, W. B. Rossow, S. L. Durden et al. (2002). 'The CLOUDSAT mission and the A-train: A new Dimension of Space-Based Observations of Clouds and Precipitation'. *Bull. Am. Meteorol. Soc.*, 83, pp. 1771–1790. DOI: 10.1175/bams-83-12-1771.

Syndergaard, S., W. S. Schreiner, C. Rocken, D. C. Hunt and K. F. Dymond (2006). 'Preparing for COSMIC: Inversion and Analysis of Ionospheric Data Products'. *Atmosphere and Climate: Studies by Occultation Methods*. Ed. by U. Foelsche, G. Kirchengast and A. Steiner. Berlin, Heidelberg: Springer Berlin Heidelberg, pp. 137–146. DOI: 10.1007/3-540-34121-8_12.

Tackett, J. L., J. Kar, M. A. Vaughan, B. J. Getzewich, M.-H. Kim, J.-P. Vernier, A. H. Omar, B. E. Magill, M. C. Pitts and D. M. Winker (2023). 'The CALIPSO version 4.5 stratospheric aerosol subtyping algorithm'. *Atmos. Meas. Tech.*, 16, pp. 745–768. DOI: 10.5194/amt-16-745-2023.

Taha, G., R. Loughman, T. Zhu, L. Thomason, J. Kar, L. Rieger and A. Bourassa (2021). 'OMPS LP Version 2.0 multi-wavelength aerosol extinction coefficient retrieval algorithm'. *Atmos. Meas. Tech.*, 14, pp. 1015–1036. DOI: 10.5194/amt-14-1015-2021.

Tarasick, D. W., H. G. J. Smit, A. M. Thompson, G. A. Morris, J. C. Witte, J. Davies, W. Davies, T. Nakano, R. van Malderen, R. Stübi et al. (2021). 'Improving ECC ozonesonde data quality: Assessment of current methods and outstanding issues'. *Earth Space Sci.*, 8, e2019EA000914. DOI: 10.1029/2019EA000914.

Tencé, F., J. Jumelet, S. Bekki, S. Khaykin, A. Sarkissian and P. Keckhut (2022). 'Australian Black Summer Smoke Observed by Lidar at the French Antarctic Station Dumont d'Urville'. *J. Geophys. Res.*, 127, e2021JD035349. DOI: 10.1029/2021JD035349.

Themens, D. R., B. Reid and S. Elvidge (2022). 'ARTIST ionogram autoscaling confidence scores: best practices'. *URSI Radio Sci. Lett.*, 4, pp. 1–5. DOI: 10.46620/22-0001.

Themens, D. R., P. T. Jayachandran, R. B. Langley, J. W. MacDougall and M. J. Nicolls (2013). 'Determining receiver biases in GPS-derived total electron content in the auroral oval and polar cap region using ionosonde measurements'. *GPS Solut.*, 17, pp. 357–369. DOI: 10.1007/s10291-012-0284-6.

Theys, N., I. De Smedt, H. Yu, T. Danckaert, J. van Gent, C. Hörmann, T. Wagner, P. Hedelt, H. Bauer, F. Romahn et al. (2017). 'Sulfur dioxide retrievals from TROPOMI onboard Sentinel-5 Precursor: algorithm theoretical basis'. *Atmos. Meas. Tech.*, pp. 119–153. DOI: 10.5194/amt-10-119-2017.

Thomason, L. W., S. P. Burton, B.-P. Luo and T. Peter (2008). 'SAGE II measurements of stratospheric aerosol properties at non-volcanic levels'. *Atmos. Chem. Phys.*, 8, pp. 983–995. DOI: 10.5194/acp-8-983-2008.

Thomason, L. W., L. R. Poole and T. Deshler (1997). 'A global climatology of stratospheric aerosol surface area density deduced from Stratospheric Aerosol and Gas Experiment II measurements: 1984–1994'. *J. Geophys. Res.*, 102, pp. 8967–8976. DOI: 10.1029/96JD02962.

Thomason, L. W., M. Kovilakam, A. Schmidt, C. von Savigny, T. Knepp and L. Rieger (2021). 'Evidence for the predictability of changes in the stratospheric aerosol size following volcanic eruptions of diverse magnitudes using space-based instruments'. *Atmos. Chem. Phys.*, 21, pp. 1143–1158. DOI: 10.5194/acp-21-1143-2021.

Todt, M. A., E. Asher, E. Hall, P. Cullis, A. Jordan, K. Xiong, D. F. Hurst and T. Thornberry (2023). 'Baseline Balloon Stratospheric Aerosol Profiles (B2SAP)—Systematic Measurements of Aerosol Number Density and Size'. *J. Geophys. Res.*, 128, e2022JD038041. DOI: 10.1029/2022JD038041.

Vaughan, G., D. P. Wareing, S. B. Jones, L. Thomas and N. Larsen (1994). 'Lidar measurements of Mt. Pinatubo aerosols at Aberystwyth from August 1991 through March 1992'. *Geophys. Res. Lett.*, 21, pp. 1315–1318. DOI: 10.1029/93gl02893.

Veefkind, J., I. Aben, K. McMullan, H. Förster, J. de Vries, G. Otter, J. Claas, H. Eskes, J. de Haan, Q. Kleipool et al. (2012). 'TROPOMI on the ESA Sentinel-5 Precursor: A GMES mission for global observations of the atmospheric composition for climate, air quality and ozone layer applications'. *Remote Sens. Env.*, 120, pp. 70–83. DOI: 10.1016/j.rse.2011.09.027.

Vernier, H., D. Quintão, B. Biazon, E. Landulfo, G. Souza, F. J. S. Lopes, N. Rastogi, R. Meena, H. Liu, S. Fadnavis et al. (2023). 'Understanding the impact of Hunga-Tonga undersea eruption on the stratospheric aerosol population using Balloon measurements, Satellite data, and model simulations'. *EGU General Assembly 2023*. Vienna, Austria: Copernicus Meetings, EGU23–6882. DOI: 10.5194/egusphere-egu23-6882.

Vernier, H., D. Quintão, B. Biazon, E. Landulfo, G. Souza, V. A. Santos, J. S. F. Lopes, C. P. A. Mendes, A. S. J. D. Matta, K. P. Damaris et al. (2025). 'Balloon Observations Suggesting Sea Salt Injection into the Stratosphere from Hunga Tonga-Hunga Ha'apai'. DOI: 10.5194/egusphere-2025-924.

Vernier, J.-P., C. Timmreck and S. Kremser (2022). *Atmospheric Impacts of the 2022 Hunga Tonga–Hunga Ha'apai Eruption: Summary of VolRes Discussion for the SSiRC Community*. Tech. rep. https://sparc-ssirc.org/downloads/VolRes_summary_of_the_Hunga-Vfinal.pdf. SPARC Stratospheric Sulfur and its Role in Climate (SSiRC) Initiative.

Vernier, J.-P., T. J. Aubry, C. Timmreck, A. Schmidt, L. Clarisse, F. Prata, N. Theys, A. T. Prata, G. Mann, H. Choi et al. (2024). 'The 2019 Raikoke eruption as a testbed used by the Volcano Response group for rapid assessment of volcanic atmospheric impacts'. *Atmos. Chem. Phys.*, 24, pp. 5765–5782. DOI: 10.5194/acp-24-5765-2024.

Vömel, H., S. Evan and M. Tully (2022). 'Water vapor injection into the Stratosphere by Hunga Tonga-Hunga Ha'apai'. *Science*, 377, pp. 1444–1447. DOI: 10.1126/science.abq2299.

Wang, H. J. R., R. Damadeo, D. Flittner, N. Kramarova, G. Taha, S. Davis, A. M. Thompson, S. Strahan, Y. Wang, L. Froidevaux et al. (2020). 'Validation of SAGE III/ISS Solar Occultation Ozone Products With Correlative Satellite and Ground-Based Measurements'. *J. Geophys. Res.*, 125, e2020JD032430. DOI: 10.1029/2020jd032430.

Wargan, K., B. Weir, G. L. Manney, S. E. Cohn, K. E. Knowland, P. A. Wales and N. J. Livesey (2023). 'M2-SCREAM: A Stratospheric Composition Reanalysis of Aura MLS Data With MERRA-2 Transport'. *Earth Space Sci.*, 10, e2022EA002632. DOI: 10.1029/2022ea002632.

Waters, J. W., L. Froidevaux, R. S. Harwood, R. F. Jarnot, H. M. Pickett, W. G. Read, P. H. Siegel, R. E. Cofield, M. J. Filipiak, D. A. Flower et al. (2006). 'The Earth observing system microwave limb sounder (EOS MLS) on the aura Satellite'. *IEEE Trans. Geosci. Remote Sens.*, 44, pp. 1075–1092. DOI: 10.1109/tgrs.2006.873771.

Winker, D. M., W. H. Hunt and M. J. McGill (2007). 'Initial performance assessment of CALIOP'. *Geophys. Res. Lett.*, 34. DOI: 10.1029/2007gl030135.

Wright, C. J., N. P. Hindley, M. J. Alexander, M. Barlow, L. Hoffmann, C. N. Mitchell, F. Prata, M. Bouillon, J. Carstens, C. Clerbaux et al. (2022). 'Surface-to-space atmospheric waves from Hunga Tonga-Hunga Ha'apai eruption'. *Nature*, 609, pp. 741–746. DOI: 10.1038/s41586-022-05012-5.

Yoon, S., A. Kotsakis, S. L. Alvarez, M. G. Spychala, E. Klovenski, P. Walter, G. Morris, E. Corrales, A. Alan, J. A. Diaz et al. (2022). 'Development and testing of a novel sulfur dioxide sonde'. *Atmos. Meas. Tech.*, 15, pp. 4373–4384. DOI: 10.5194/amt-15-4373-2022.

Young, S. A. and M. A. Vaughan (2009). 'The Retrieval of Profiles of Particulate Extinction from Cloud-Aerosol Lidar Infrared Pathfinder Satellite Observations (CALIPSO) Data: Algorithm Description'. *J. Atmos. Ocean. Tech.*, 26, pp. 1105–1119. DOI: 10.1175/2008JTECHA1221.1.

Young, S. A., M. A. Vaughan, R. E. Kuehn and D. M. Winker (2013). 'The Retrieval of Profiles of Particulate Extinction from Cloud–Aerosol Lidar and Infrared Pathfinder Satellite Observations (CALIPSO) Data: Uncertainty and Error Sensitivity Analyses'. *J. Atmos. Ocean. Tech.*, 30, pp. 395–428. DOI: 10.1175/jtech-d-12-00046.1.

Yu, W., R. Garcia, J. Yue, A. Smith, X. Wang, W. Randel, Z. Qiao, Y. Zhu, V. L. Harvey, S. Tilmes et al. (2023). 'Mesospheric temperature and circulation response to the Hunga Tonga-Hunga-Ha'apai volcanic eruption'. *J. Geophys. Res.*, 128, e2023JD039636. DOI: 10.1029/2023JD039636.

Zawada, D. J., L. A. Rieger, A. E. Bourassa and D. A. Degenstein (2018). 'Tomographic retrievals of ozone with the OMPS Limb Profiler: algorithm descrip-

tion and preliminary results'. *Atmos. Meas. Tech.*, 11, pp. 2375–2393. DOI: 10.5194/amt-11-2375-2018.

Zhang, C., C. Hu, S. Shang, F. E. Müller-Karger, Y. Li, M. Dai, B. Huang, X. Ning and H. Hong (2006). 'Bridging between SeaWiFS and MODIS for continuity of chlorophyll-a concentration assessments off Southeastern China'. *Remote Sens. Environ.*, 102, pp. 250–263. DOI: 10.1016/j.rse.2006.02.015.

Zhu, Y., H. Akiyoshi, V. Aquila, E. Asher, E. M. Bednarz, S. Bekki, C. Brühl, A. H. Butler, P. Case, S. Chabrillat et al. (2025). 'Hunga Tonga–Hunga Ha'apai Volcano Impact Model Observation Comparison (HTHH-MOC) project: experiment protocol and model descriptions'. *Geosci. Model Dev.*, 18, pp. 5487–5512. DOI: 10.5194/gmd-18-5487-2025.

Zou, C.-Z. and H. Qian (2016). 'Stratospheric Temperature Climate Data Record from Merged SSU and AMSU-A Observations'. *J. Atmos. Ocean. Tech.*, 33, pp. 1967–1984. DOI: 10.1175/JTECH-D-16-0018.1.

Zou, C.-Z., H. Qian, W. Wang, L. Wang and C. Long (2014). 'Recalibration and merging of SSU observations for stratospheric temperature trend studies'. *J. Geophys. Res.*, 119, pp. 13, 180–13, 205. DOI: 10.1002/2014JD021603.